海洋安全學會誌 第3卷 第1號, pp. 1~14, 1997. 1.

論 文

A Study on the Collision and Grounding of Ships using HYDROCODE LS/DYNA3D

Lee, Sang-Gab* · Chung, Young-Gu**

HYDROCODE LS/DYNA3D를 이용한 선박의 충돌 및 좌초에 관한 연구

이 상 갑* · 정 영 구**

〈Contents〉

Abstract

This paper describes a series of numerical simulations of collision between a 310,000 DWT double hull VLCC (struck ship) and three 35,000, 70,000 and 105,000 DWT tankers (striking ships) using LS/DYNA3D. Collisions are assumed to occur at the middle of the VLCC with the striking ships moving at right angle to the VLCC centerline. Striking ship speeds are varied to find a critical speed without failure of inner side shell, and the informations of collision force and absorption energy of each case are also reported. The validation of LS/DYNA3D in this study was made by comparing the result of numerical simulation of LS/DYNA3D with that of double hull tanker grounding experiment by the Carderock Division of Naval Surface Warfare Center(CDNSWC).

* 정 회 원, 한국해양대학교 조선해양공학부 부교수
** 학생회원, 한국해양대학교 대학원 박사과정

요 약

이 논문에서는 LS/DYNA3D을 사용하여 31만톤 초대형 이중선체 유조선(피충돌선)과 3만5천톤, 7만톤, 10만5천톤의 각각 3가지 형태의 유조선(충돌선)들과의 일련의 충돌 수치 시뮬레이션에 대하여 기술하고 있다. 여기에서는 초대형 유조선의 중앙부에 충돌선들이 횡방향으로 수직하게 충돌이 일어나는 것으로 가정한다. 이 논문에서는 선측내판이 찢어지지 않는 충돌선들의 임계속도와, 또한 각 경우에 대한 충돌력 및 흡수에너지에 관한 정보들을 구하고자 한다. 그리고 본 논문에서 사용되는 시뮬레이션 LS/DYNA3D는 CDNSWC에서 수행한 이중선체 유조선의 좌초실험의 결과와 LS/DYNA3D의 수치해석의 결과를 비교하여 검증하였다

1. Introduction

From departure of the study on ship hull resistance to collision of nuclear powered merchant ships in the late 1950s, Minorsky[1] presented a formula to estimate absorbed energy in collision based on data of 25 collisions provided by the US Coast Guard. Studies have been extensively performed by many researchers. Since the grounding of Exxon Valdez in 1989 focused the international attention on the oil spills, the United States of America required a double hull for future tankers in 1990 and IMO adopted similar, though a little bit relaxed regulations in 1992. Further research is necessary to come up with design regulations and recommendations for tanker design to reduce the risk of oil spilling.

In structural design and optimization of a double hull tanker, it is important to have a good understanding of the behavior of its structure in collision and grounding, and to have an accurate prediction of its hull resistance against collision and grounding in terms of energy absorption capacity and resulting damage[2]. Since the ruptures of inner side shell and inner bottom shell due to collision and grounding and/or stranding are critical failure modes, the informations on the energy absorption capacity up to the above failures might be used as a basis to design and to optimize the structure of double hull tankers.

While simplified methods to estimate the energy absorption capacity in collision are proposed[3,4], since many years, hydrocodes such as MSC/DYTRAN, LS/DYNA3D and PAM-CRASH have been successfully used to simulate high-speed highly nonlinear phenomena in defense, safety and space development such as impact, crash, penetration and explosion. These hydrocodes were applied to ship collisions in inland water ways[5], and to simulate full scale collision experiments using a decoupled fluid-structure three step approach[6] and a coupled fluid-structure simulation[7]. Full scale numerical simulations of collision for double hull VLCCs were also carried out using MSC/DYTRAN or LS/DYNA3D to clarify the behavior of different structural members and to suggest a new design of VLCC side structures during failure as well as energy absorption mechanism[8-12]. Such a full scale numerical simulation may provide an accurate predictions on energy absorption capacity and failure modes of real-sized ship structures.

It is desirable to estimate the crashworthiness of ship structures against collision comparing their energy absorption capacities with each

other. For this study, several sizes of striking ships with different collision speed are used to collide against each struck VLCC up to failure of inner side shell. This paper describes a series of numerical simulations of collisions between one type of 310,000 DWT VLCC (struck ship) and three types of 35,000, 70,000 and 105,000 DWT tankers(striking ships) using LS/DYNA3D. Collision are assumed to occur at the middle of the VLCC with the striking ships moving at right angle to the VLCC centerline. Collision speeds of each striking ship are varied to find a critical failure modes, and informations of collision force and absorbed energy of each case are also reported.

2. Validation of LS/DYNA3D

To validate LS/DYNA3D to use in this study, it is desirable to compare the result of numerical simulation of LS/DYNA3D with experimental one. Several large scale oil tanker grounding experiments have been performed by the Carderock Division of Naval Surface Warfare Center (CDNSWC) as part of the Advanced Double Hull Technology Project[13]. The first experiment represented a conventional T-5 Paul Buck double hull tanker bottom with transverse and longitudinal framing, which provided baseline information for comparison purposes in both numerical analyses and experiments.

Figure 1 shows geometry and construction details for the conventional double hull structure in the 30,000~40,000 ton range at approximately one fifth scale, which consists of the double bottom structure beneath one oil tank, the forward and aft transverse bulkheads, and heavy sideplates. The material used for the grounding model was ASTM A569 with the measured yield and ultimate stresses of 282 MPa and 344 MPa, respectively.

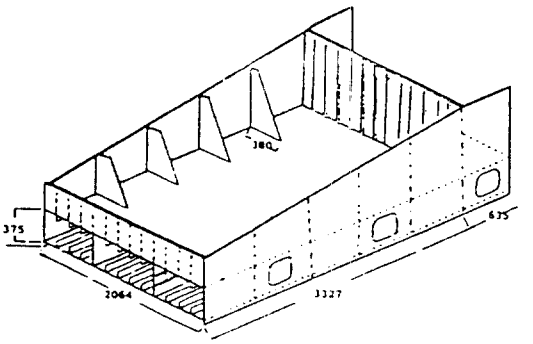

Fig. 1 Dimension of grounding model[13]

A series of large scale oil tanker grounding experiments have been conducted using the Grounding Test Machine, which consisted of a 227 tonne test vehicle (or sled) and impact area. Sled built on twin railcars carried the grounding model down an inclined set of railroad tracks to an impact area at a sled velocity of 6.1 m/sec (12 knots). A steel grounding rock included in the impact area was a 914 mm high, 90 degree cone with a 178 mm radius spherical tip. The installation and orientation of the inclined grounding model is shown in Fig. 2 with 7.4 degrees of attack angle and the entry/exit height of the rock tip.

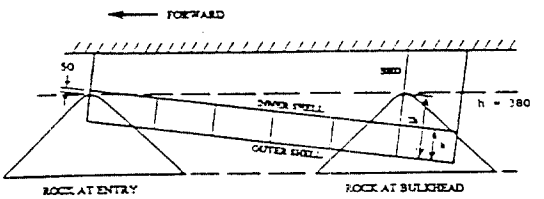

Fig. 2 Installation of grounding model[13]

Figure 3(a) shows the plots of the finite element mesh of grounding double hull

structure and grounding rock. All members of inner and outer shells, transverse and longitudinal webs, forward/aft bulkheads, small stiffeners, and grounding rock are modeled using around 18,000 shell element. The mass of the sled is controlled by rigid plate on the top of the double hull model, which is invisible in Fig. 3. The grounding rock is modeled to be rigid and the double hull model is restrained to move straightly forward, and not upward/downward.

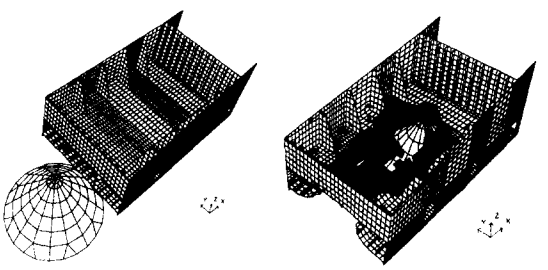

(a) (b)

Fig. 3 Finite element mesh and rupture configuration of grounding model

Two kinds of material types are employed for numerical simulation: strain rate dependent isotropic plasticity for the grounding double hull model and isotropic plasticity for the grounding rock. The former material type is suitable for the consideration of the material dynamic effect. Dynamic yield stress, $\sigma_Y = \sigma_o\{1+(\dot{e}/D)^{1/p}\}$, is used [14], where σ_o is static yield stress, $\dot{e}$ is stain rate, and $D(=40.4\,s^{-1})$ and $p(=5)$ are constants. The density and Poisson's ratio to use here are 7850 kg/m3 and 0.3, respectively. Every finite element is due to be eliminated when plastic strain reaches to the failure value, 0.25 in this study.

Figure 3(b) shows the configuration of rupture process of the grounding model by the grounding rock. Figure 4 shows the comparison of numerical simulation result with NSWC experimental one about the horizontal impact force (plate resisting force) vs. the sled position. Compared to the experimental result, it can be said that the numerical simulation result is satisfactory and that the already acknowledged tool LS/DYNA3D is sufficient to perform the following collision problems.

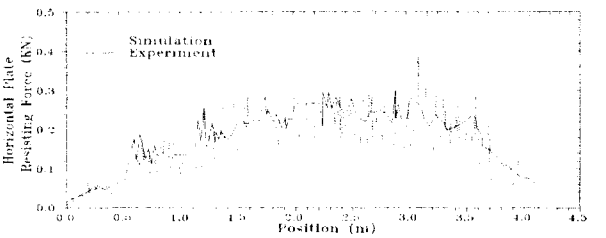

Fig. 4 Comparison of numerical simulation and NSWC experimental results

3. Collision Scenarios and Simulation Models

3.1 Collision scenarios

In the considered struck ship, 310,000 DWT D/H VLCC, three tanks are installed across its breadth inside the double hull, cross ties (struts) are fitted in the side tanks and three side stringers are also fitted in the double side, as shown Fig. 5. When the side of struck ship is hit by the striking ship, cross ties transfer the impact force to the side longitudinal bulkhead. It was reported that the side longitudinal bulkhead showed elastic deformation behavior even while cross ties failed[9]. Collision scenarios considered in this study are shown in Table 1, where striking ships collides against a stationary struck ship in each collision scenario as shown in Fig. 5.

Table 1 Collision Scenarios

Struck Ship 310,000 DWT	Striking Ship					
	35,000 DWT		70,000 DWT		105,000 DWT	
	5.5 knots	I	4.5 knots	III	4.00 knots	VI
	6.0 knots	II	5.0 knots	IV	4.25 knots	VII
			5.0 knots(u)	V		

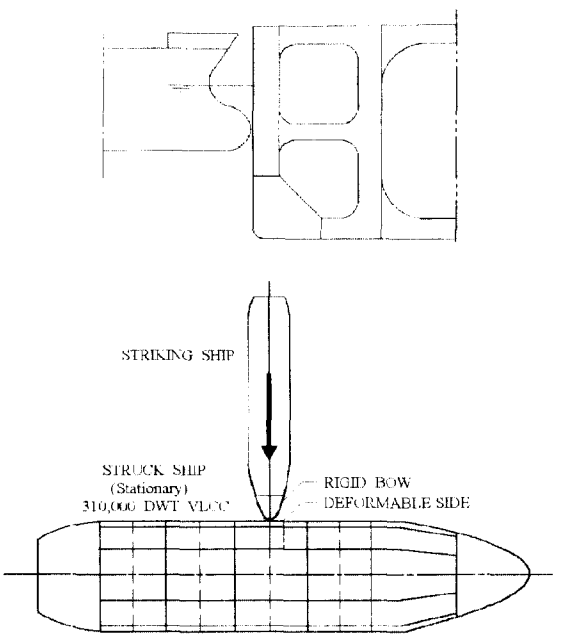

Fig. 5 Numerical model outline

3.2 Struck and striking ships models

In a high energy collision, large plastic deformations take place in the location of collision on the struck and/or the striking ships, while the rest of both ships show different levels of elastic deformations. Compared to the plastic deformations in the location of collision, the elastic deformations are very small and may be neglected. Therefore, only the regions in both ships containing members expected to show the plastic deformations are modeled as deformable structures, and the rest of both ships, as rigid bodies.

In full scale simulations during collision using MSC/DYTRAN [9], the side of the struck VLCC in the location of collision as well as the bows of the striking ships were modeled as deformable structures, and the reset of the ships, as rigid bodies. The water around the VLCC was modeled with an Eulerian finite volume mesh, and ALE(Arbitrary Lagrangian Euler) coupling was used to couple the water effect to the VLCC. Their results showed that the motions of both striking ship and struck ship were very small with heavy struck ship, and that the effect of the fluid around the struck ship was also small. Damage of the bow of the striking ship was also reported to be relatively smaller than that of the VLCC side[8,9].

By these results of full scale simulations, in this paper, the effect of the fluid around the struck ship is neglected. Only the deformable structure of the struck ship is employed and the rest of struck ship is neglected. On the assumption that the position of collision is the middle of cargo hold at the center of struck ship, in the longitudinal direction the deformable structure is modeled from the center of struck ship to the two web frames and a symmetric condition is established at the center of cargo hold, as shown in Fig. 5. In the transverse direction, the side longitudinal bulkhead is not modeled due to the level of elastic deformations until the failure of cross ties. Web frame and the shells of deck, bottom and inner bottom connected to the side longitudinal bulkhead are constrained to the transverse direction. Since damage of the bow of the striking ship was relatively smaller than that of the VLCC side, the bow of the striking ship is modeled as rigid

body in this study.

Figure 6 shows the structural members of struck ship VLCC, such as outer side shell, inner side shell, longitudinal stiffener of outer side shell, longitudinal stiffener of inner side shell, No. 1 web, No. 2 web, No. 3 web, No. 1 stringer, No. 2 stringer, No. 3 stringer, No. 1 cross tie, No 2 cross tie, No. 3 cross tie, deck, etc..

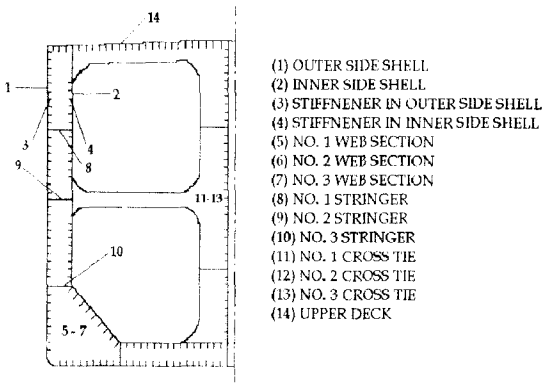

Fig. 6 Structural members of struck VLCC

Figure 7(a) shows the plots of the finite element mesh of the side of struck ship, where the breadth of side double hull is 3.38 m and the space of web section is 5.08 m. The bow of 35,000 DWT striking ship collides against the center of cross tie and its upper deck is located below that of the struck VLCC(scenarios Ⅰ, Ⅱ), as shown in Fig. 7(b). On the other hands, the center of the bow of 70,000 DWT striking ship hits a little bit below the center of cross tie and its upper deck is located the same level as that of the struck VLCC(scenarios Ⅲ, Ⅳ), shown in Fig. 7(c). For consideration of the effect on the location of the upper deck of striking ship to that of the struck VLCC, scenarios Ⅴ is included in this study, such that the upper deck of 70,000 DWT striking ship is located above that of the struck VLCC, not shown in Figures. In the case of 105,000 DWT striking ship strikes much below the center of cross tie and its upper deck is also located above that of the struck VLCC(scenarios Ⅵ, Ⅶ), as shown in Fig. 7(d). All members of shells, web frames, longitudinal stiffeners, and stringers are modeled using shell element. Around 12,000 shell elements are used in this study.

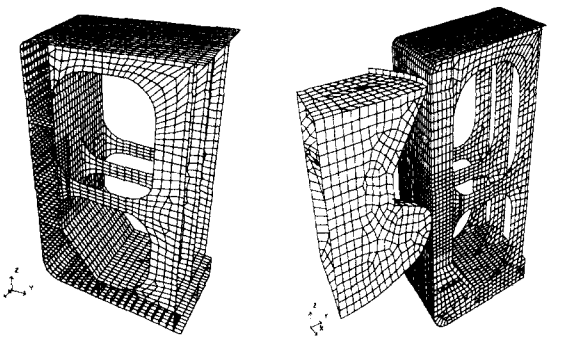

(a) Finite element mesh (b) 35,000 DWT

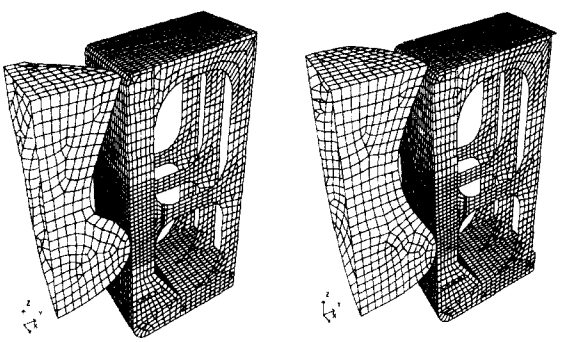

(c) 70,000 DWT (d) 105,000 DWT

Fig. 7 Finite element mesh of deformable side of struck VLCC and 3 striking ships

Elastoplastic material with nonlinear strain hardening and strain rate effects are used, and the properties are as follows:

Density	7850.0 Kg/m^3
Modulus of elasticity	210 GPa
Poisson ratio	0.3
Yield stress(mild steel)	250 MPa
Ultimate stress(mild steel)	400 MPa
Constants of Cowper Symonds Eq.	40.4, 5.0
Failure plastic strain	0.2

In collision, tearing of weld lines is usually observed in areas where large damage occurs. Modeling of weld lines and their failure may be necessary in order to accurately predict collision damage. When stresses acting on the weld satisfy a predefined failure condition, the joint breaks up and internal forces are unloaded to the surrounding structure. Since every shell element is complied with failure plastic strain, weld lines are to be neglected in this study.

In the plane of symmetry, grid points on continuous longitudinal members of the struck ship and the center plane of the striking ship are given symmetric boundary conditions ($U_x = \theta_y = \theta_z = 0.0$). The web frame in the symmetric plane of the struck ship model must contribute only half of its strength to the model. Instead of installation of the side longitudinal bulkhead of the struck ship as the boundary condition, all nodal points at that plane are constrained to the transverse direction. Because of symmetry, only one half of rigid body of bow is explicitly modeled, and the total mass of the striking ship together with 10% added virtual mass is distributed.

4. Results of Simulation

Simulations of the seven scenarios have been carried out, and their results are summarized as follows:

4.1 Collision scenarios Ⅰ & Ⅱ

Figure 8 shows the deformation and rupture plots of VLCC side with collision speed 6 knots (scenario Ⅱ) (a) after the failure in the outer side shell, (b) before the failure in the inner side shell, (c) after the failure in the inner side shell. Figure 8(d) is another one of Fig. 8(c) from different viewpoint. The bulbous bow penetrates the outer side shell, then the inner side shells at the cross tie of center web frame. It is interesting that the buckling mode of No. 1 cross tie in the tank changes during collision. At the initial stage No. 1 cross ties buckle mainly in bending mode as shown in Fig. 8(a), and at the last stages in Figs. 8(c) and (d) the torsional mode of No. 1 cross tie near the collision position can be observed. Since the deck of striking ship collides against the top outer side shell of struck VLCC, its deck penetrates the outer side and inner side shells without rupture of the upper deck of the struck VLCC during collision.

The bulbous bow of striking ship with collision speed 5.5 knots(scenario Ⅰ) pierces the outer side shell and rebounds after the bow arrives at maximum 0.215 m ahead of the inner side shell without rupture of inner side shell. Scenario Ⅰ shows almost the same trend in the deformation and rupture configuration, and equivalent plastic contour plots as those of Figs. 8(a) and (b).

Figure 9 shows the variation of collision force with time and penetration in scenarios Ⅱ. It can be seen that failure of the outer side shell starts at time 0.15 sec and the inner side shell initiates to be torn away at time 1.79 sec with maximum deformation, 0.85 m, of the inner side shell.

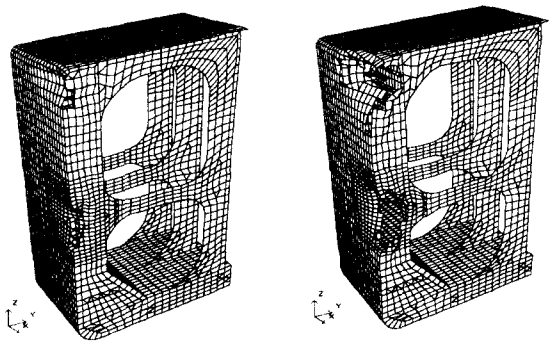

(a) time = 0.5 sec (b) time = 1.5 sec

(c) time = 3.0 sec (d) time = 3.0 sec

Fig. 8 Deformed side structure in scenario II

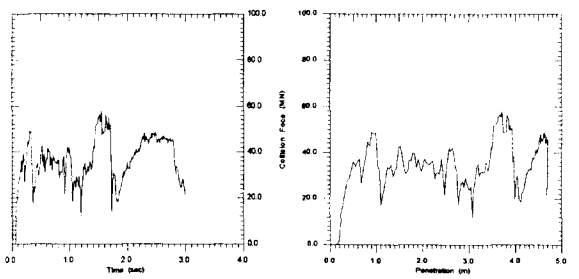

Fig. 9 Collision force variation in scenario II

Figure 10 shows the variation of the total absorbed energy with time and with penetration in scenario I and II. It can be seen that the absorbed energy arrives at 159.6 MN-m when the inner side shell begins to be torn away in scenario II. It might be thought, therefore, that the critical absorbed energy has to be larger than at least 159.6 MN-m to rupture the inner side shell with 35,000 DWT striking ship at the same position of collision to the struck VLCC as the scenarios I and II.

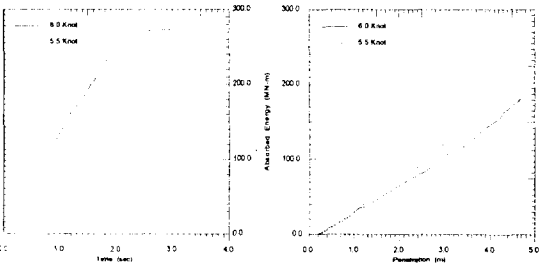

Fig. 10 Total absorbed energy in scenarios I and II

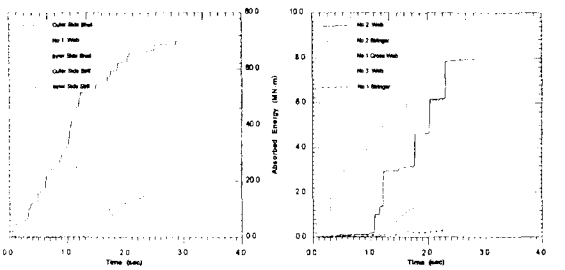

Fig. 11 Energy distribution in scenario II

Figure 11 shows the absorbed energy distribution of each member with time in scenario II. Most of absorbed energy are carried by outer side shell, No. 1 web, inner side shell, longitudinal stiffeners of outer and inner side shells, No. 2 web, and No. 2 stringer in capacity sequently during collision, while deck does not contribute to collision in this scenario. This might be due that the deck of the striking ship collides against below the deck of the struck VLCC.

4.2 Collision scenarios Ⅲ, Ⅳ & Ⅴ

Figure 12 shows the deformation and rupture plots of VLCC side with collision speed 5.0 knots (scenario Ⅳ) (a) after the failure in the outer side shell, (b) before the failure in the inner side shell, (c) right after the failure in the inner side shell. Figure 12(d) is another one of Fig. 12(c) from different viewpoint. In this case the bulbous bow penetrates the outer side shell then the inner side shell just below the cross tie of the center web frame. The corner part between the deck and the top outer side shell of the struck VLCC is ruptured and folded. Compared to the case of scenario Ⅱ, the buckling modes of No. 1 and 2 cross ties apparently occur after the rupture of outer side shell, which is due to the larger contact area of bulbous bow of 70,000 DWT striking ship than that of 35,000 DWT one. Similar to the case of scenario Ⅱ, the torsional modes of No. 1 and 2 cross ties can be observed at the last stages, as shown in Figs. 12(c) and (d).

The bulbous bow of striking ship with collision speed 4.5 knots (scenario Ⅲ) penetrates the outer side shell and rebounds after the bow arrives the inner side shell without rupture of inner side shell. Scenario Ⅲ shows almost the same trend in the deformation plots as those of Figs. 12(a) and (b). As can be expected from the scenario Ⅴ, the corner part between the upper deck and the top outer side shell of the struck VLCC is more ruptured and compressed than the case in scenario Ⅳ, while the bulbous bow of the striking ship penetrates the outer side shell and rebounds after the bow arrives the inner side shell without rupture of inner side shell like scenario Ⅲ.

Figure 13 shows the variation of collision force with time and penetration in scenario Ⅳ.

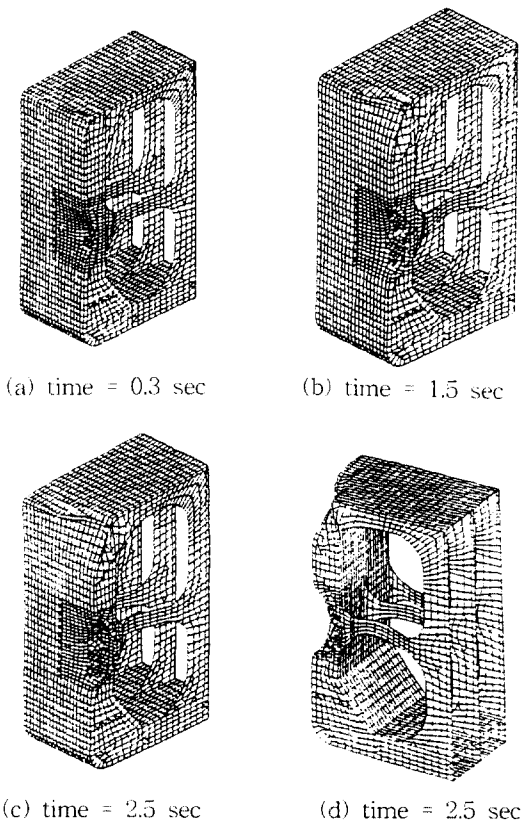

(a) time = 0.3 sec (b) time = 1.5 sec

(c) time = 2.5 sec (d) time = 2.5 sec

Fig. 12 Deformed side structure in scenario Ⅳ

It can be seen that the failure of the outer side shell starts at time 0.16 sec and the inner side shell initiates to be torn away at time 2.45 sec with maximum deformation, 1.5 m, of the inner side shell. Compared to scenario Ⅱ in Fig. 9, it can be seen that the maximum collision force of scenario Ⅳ is larger than that of scenario Ⅱ.

Figure 14 also shows the variation of the total absorbed energy with time and penetration in scenarios Ⅲ to Ⅴ. It can be seen that the absorbed energy arrives at 247.5 MN-m when the inner side shell begins to be torn away in scenario Ⅳ. The same conclusion as the scenario Ⅱ can be drawn that the critical absorbed energy has to be greater than at least 247.5 MN-m

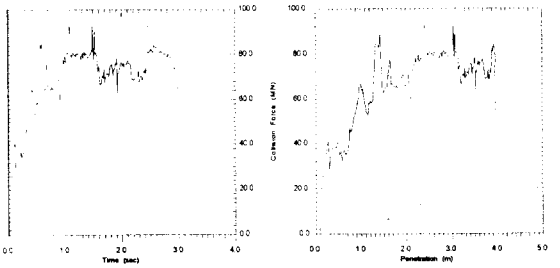

Fig. 13 Collision force variation in scenario Ⅳ

with 70,000 DWT striking ship at the same position of collision to the struck VLCC as scenarios Ⅳ. Almost the same trends can be found between scenarios Ⅲ and Ⅳ, as shown in Fig 14, while different tendencies, between scenarios Ⅳ(Ⅲ) and Ⅴ. The absorbed energy of scenario Ⅲ is much smaller than those of scenarios Ⅳ and Ⅴ. Even though the absorbed energy of scenario Ⅴ is a little bit small than that of scenario Ⅳ, inner side shell of the former does not rupture. This might be the effect on the collision location of the upper deck of striking ship against struck ship. The collision of the upper deck of striking ship might reduce the portion of the absorbed energy of the bulbous bow of striking ship as its upper deck climbs the corner between the upper deck and the top outer side shell of struck ship.

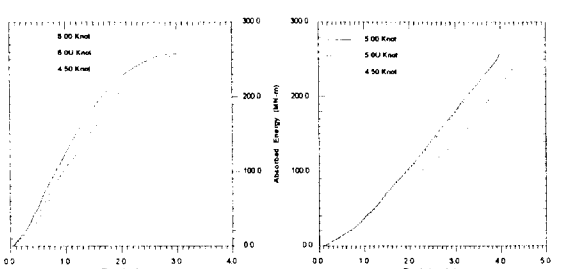

Fig. 14 Total absorbed energy in scenarios Ⅲ to Ⅴ

Figure 15 shows the absorbed energy distribution of each members with time in scenario Ⅳ. Similar to the trends of scenario Ⅱ, most of absorbed energy is carried by outer side shell, No. 1 web, longitudinal stiffener of outer side shell, No. 2 and No 3 webs in capacity sequently. Compared to the case of scenario Ⅱ, the inner side members, such as inner side shell and longitudinal stiffener of inner side shell, do not much contribute to the collision, while the deck member does, much. Outer side shell and No. 1 web in scenario Ⅳ is much larger absorbed energy (almost 1.5 times) than those of scenario Ⅱ.

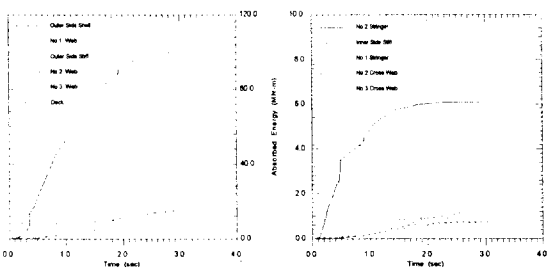

Fig. 15 Energy distribution in scenario Ⅳ

4.3 Collision scenarios Ⅵ & Ⅶ

Figure 16 shows the deformation and rupture plots of VLCC side with collision speed 4.25 knots (scenario Ⅶ) (a) at the onset of the failure in the outer side shell, (b) before the failure in the inner side shell, (c) right after the failure in the inner side shell. Fig. 16(d) is another deformation and equivalent plastic strain contour plots from different viewpoint of Fig. 16(c). The bulbous bow of striking ship crashes the outer side shell between cross tie and hopper tanker, and the upper deck of striking ship collides upward against the deck of struck VLCC like scenario Ⅴ. The scope of rupture at the corner between upper deck and top outer side shell of the struck VLCC is much smaller than those of scenarios Ⅱ and Ⅳ.

While the local rupture in the struck VLCC

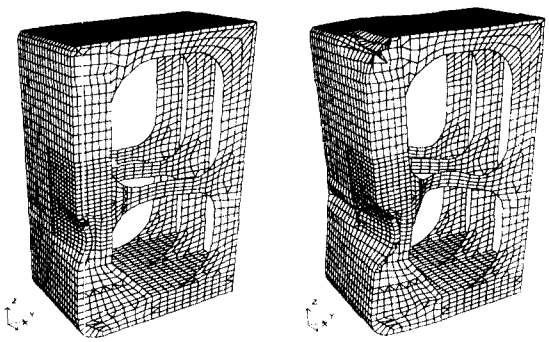

(a) time = 0.55 sec (b) time = 2.0 sec

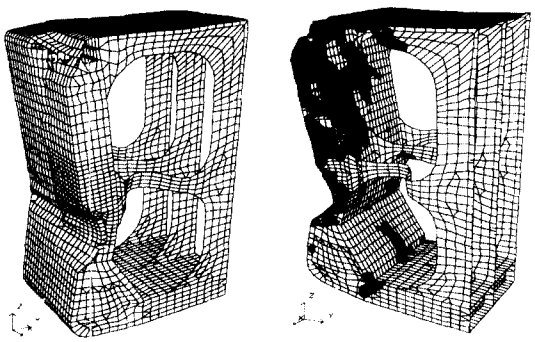

(c) time = 2.3 sec (d) time = 2.3 sec

Fig. 16 Deformed side structure (scenario Ⅶ)

occurs in scenario Ⅱ, the global damage and rupture happen to in scenario Ⅶ. Besides the failure in the inner side shell around the cross tie in scenario Ⅶ, the rupture can be found in the conjunction with hopper tank and inner bottom shell. All cross ties of the struck VLCC buckles more seriously than those of scenarios Ⅱ and Ⅳ, as shown in Fig. 16. Compared to the cases of scenarios Ⅱ and Ⅳ, the buckling modes of all cross ties occur during rupture of the outer side shell, as shown in Fig. 17(a), which is due to the more larger contact area of bulbous bow of 105,000 DWT striking ship than those of 35,000 and 70,000 DWT ones. Extreme bending and torsional buckling modes in all cross ties can be found during the rupture of inner side shell, as shown in Fig. 17(b).

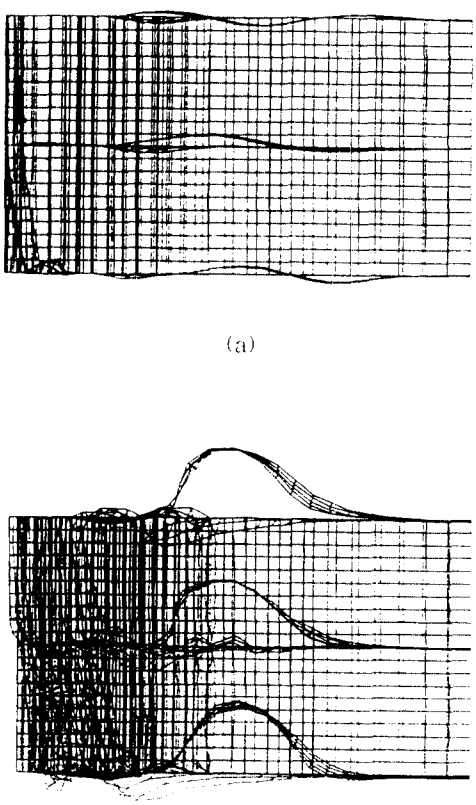

(a)

(b)

Fig. 17 Buckling modes from deck in scenario Ⅶ

Figure 18 shows the variation of collision force with time and penetration in scenario Ⅶ. It can be seen that the failure of the outer side shell starts at time 0.55 sec and that of the inner side shell, at time 2.28 sec with maximum deformation, 2.4 m, of the inner side shell. The

maximum collision force in this case is almost the same as that of scenario Ⅳ, and is much larger (almost 2 times) than that of scenario Ⅱ. It is known that mass of the striking more dominates the collision force than its collision speed does, even though scenarios Ⅳ and Ⅶ have about 1.4~1.5 times as large as scenario Ⅱ in intial kinetic energy. This fact does not hold good in scenarios Ⅳ and Ⅴ, which might be the effect of the collision location of upper deck of striking ship against the corner between the top outer side shell and the deck of struck VLCC. And another effect is the flexibility of impact position of struck VLCC, such as the location between hopper tanker and cross tie of the struck VLCC.

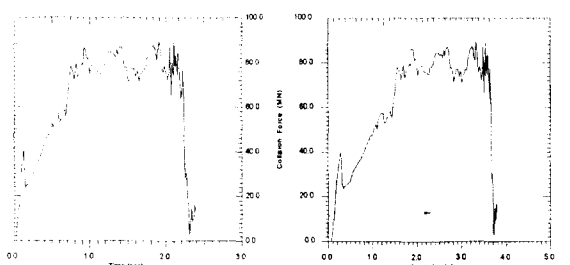

Fig. 18 Collision force variation in scenario Ⅶ

The variation of the total absorbed energy with time and penetration in scenarios Ⅵ and Ⅶ can be found in Fig. 19. In this case the bulbous bow of striking ship reaches the inner side shell with rupture beyond 230.0 MN-m.

Figure 20 shows the absorbed energy distribution of each members with time in scenario Ⅶ. Most of absorbed energy are carried by outer side shell, No. 1 web, No. 2 web, No. 3 web, longitudinal stiffeners of outer side shell, deck, No. 3 stringer, No. 2 stringer, and longitudinal stiffeners of inner side shell in capacity sequentially. The contribution of outer side shell in scenario Ⅶ is less than that of scenario Ⅳ, and the others are almost the same level as those of scenario Ⅳ.

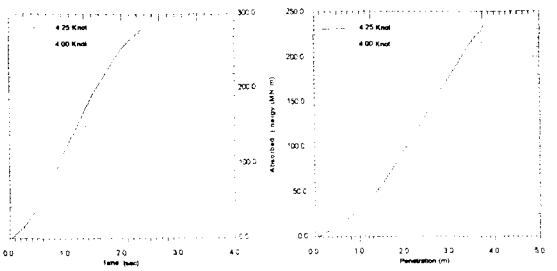

Fig. 19 Total absorbed energy in scenarios Ⅵ and Ⅶ

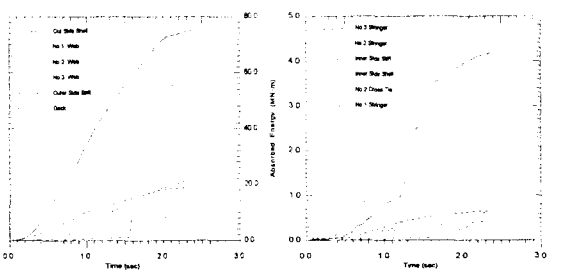

Fig. 20 Energy distribution in scenario Ⅶ

5. Conclusions

Full scale numerical simulations of collision for the struck 310,000 DWT double hull VLCC with three striking 35,000, 70,000 and 105,000 DWT tankers were presented using LS/DYNA3D, to figure out the critical failure modes and the informations of collision force and absorbed energy of each case. It might be thought that it was useful to use full numerical simulation to assess the structural failure and energy absorption capacity of VLCC in collision, for which large or full scale experiments are difficult and not practical.

It has been observed that the structural

failure behavior and the absorbed energy greatly depend on the location of collision on the side structure(collision contact direction between striking and struck ships, flexibility of struck ship structure at collision region) and shape of sticking ship(collision contact area), besides the mass and speed of striking ship.

According to the numerical simulations of this study, the critical collision speeds of 310,000 DWT struck VLCC can be estimated just below 6.0 knots for 35,000 DWT, about 5.0 knots for 70,000 DWT, and about 4.25 knots for 105,000 DWT striking ships. Intial kinetic energy is increased as the mass of striking ship is increased, where the initial kinetic energy of 70,000 DWT of striking ship with speed 5.0 knots is about 1.4 times as large as that of 35,000 DWT one with speed 6.0 knots, and 105,000 DWT one with speed 4.25 knots, about 1.5 times.

As expected, the collision force of 35,000 DWT of striking ship is much less than those of 70,000 DWT and 105,000 DWT ones, and the absorbed energy of the former for fracture of inner side shell is much less than those of the latter. While the local rupture in struck VLCC occurs at the collision with relative small striking ship (35,000 DWT), the global damage and rupture happen to at the collision with large one (105,000 DWT). From these results, the following comment might be obtained that this type of 310,000 DWT struck VLCC has the failure modes in the inner side shell with lower absorbed energy from local rupture (30,000 DWT) than from global deformation and rupture (105,000 DWT) during collision.

Structural members, such as outer side shell and No.1 web of 310,000 DWT struck VLCC sustain almost the absorbed energy. As the local rupture occurs rather than the global deformation and rupture, the inner members, such as inner side shell and longitudinal stiffener of inner side shell, support the absorbed energy partly.

For the future study, realization of optimized double hull/ bottom as well as estimation of its critical (limit) collision/ grounding resistance in collision/grounding will be performed, through the simulations using more various cases and single parametric factor, while more complex factors are considered simultaneously in this study.

Acknowledgements

This paper was supported (in part) by NON DIRECTED RESEARCH FUND, Korea Research Foundation. The authors acknowledge the support of this work.

References

1. V. U. Minorsky, "An analysis of ship collision with reference to protection of nuclear power plants", J. of Ship Research, 1959.
2. J. Amdahl and D. Kavile, "Analysis and design of ship structures for grounding and collision", PRADS '92, 1992.
3. H. Ito, K. Kondo, N. Yoshimura, M. Kawashima and S. Yamamoto, "A simplified method to analyze the strength of double hulled structures in collision(3rd report)", SNAJ, Vol. 160, 1986.
4. S. Valsgard and E. Pattersen, "Simplified nonlinear analysis of ship/ship collisions", Norwegian Maritime Research, No. 3, 1982.
5. H. Lenselink, K.G. Thung, H.L. Stipdonk and P.J. van der Weijde, "Numerical simulation of ship collisions", ISOPE-92,

San Francisco, June 1992.

6. H. Lenselink and K.G. Thung, "Numerical simulations of the Dutch-Japanese full scale ship collision tests", The conference on prediction methodology of tanker structural failure, Tokyo, July 1992.
7. H. Lenselink et. al., "A 3-dimensional numerical simulation of the full scale Dutch-Japanese full scale ship collision tests with ALE fluid-structure interaction", FEM WORLD CONFERENCE, Monte Carlo, November 1993.
8. J.Y. Kim, K.J. Lee, J.M. Kang, D.H. Kim, S. Rashed and D. Xiang, "Behavior of double hull VLCCs in collision", PRADS '95, September 1995.
9. Jungsin Che and Gibok Jang, "Numerical simulation of structural response of D/H VLCC in collision", PRADS '95, September 1995.
10. Atsushi Sano, et. al., "A study on the strength of double hull side structure of VLCC in collision", MARIENV'95, September 1995.
11. Takao Kuroiwa, et. al., "Numerical simulation of collision and grounding of ships", MARIENV'95, September 1995.
12. Ou Kitamura, "Comparative study on collision resistance of side structuer", Int. Conference on Designs and Methodologies for Collision and Grounding Protection of Ships, August 1996.
13. James L. Rodd and Jerome P. Sikora, "Double hull grounding experiments", Proc. of the 5th ISOPE Conference, The Hague, The Netherlands, June 1995.
14. G.R. Cowper and P.S. Symonds, "Strain-Hardening and Strain-Rate Effects in the Impact Loading of Cantilever Beams", Tech. Report No. 28, Brown University, Rhode Island, 1957.